

Supporting Information

Enhanced oxygen evolution activity on mesoporous cobalt-iron oxides

Tianmi Tang, Qiaoqiao Zhang, Xue Bai, Zhenlu Wang, and Jingqi Guan*

Institute of Physical Chemistry, College of Chemistry, Jilin University, 2519 Jiefang Road, Changchun 130021, P. R. China.

*E-mail: guanjq@jlu.edu.cn (J.Q. Guan)

Experimental section

Materials

All chemicals were analytical grade and were used as purchased without further purification. Solutions were prepared using high purity water (Millipore Milli-Q purification system, resistivity > 18 M Ω ·cm).

Synthesis of SBA-15 and mesoporous cobalt-iron oxides

Synthesis of SBA-15

SBA-15 was prepared according to the literature.¹ In a typical synthesis, Pluronic P123 (2 g) was first dissolved in 15 mL of H₂O and 60 mL of 2 M HCl, and then 4.68 mL (0.02 mol) of TEOS was added under stirring at 40 °C. The molar composition of the mixture, TEOS/P123/HCl/H₂O, was 1/0.017/6/192. Thereafter, the mixture was

maintained under stirring at 40 °C for 24 h and then it was transferred into an autoclave to age for 24 h at 100 °C under static conditions. Finally, the sample was filtered, washed with distilled water thoroughly, air-dried, and calcined at 550 °C to remove the template. The dry white solid was denoted as SBA-15.

Synthesis of mesoporous cobalt-iron oxides

0.5 g of SBA-15 was dispersed in 50 mL of toluene at 65 °C. Then, 0.68 g of cobalt nitrate hexahydrate and 0.047 g of iron nitrate nonahydrate were added into this mixture along with forceful stirring for 3 h. After filtrating, the obtained pink powders were calcined at 400 °C for 2 h. The SBA-15 template was removed by washing with 2 M of hot NaOH solution, and mesoporous $\text{CoFe}_{0.05}\text{O}_x$ without template was finally obtained, which was denoted as meso- $\text{CoFe}_{0.05}\text{O}_x$.

For comparison, mesoporous iron-cobalt oxides with different Fe/Co ratios (i.e. 0.01/1, 0.025/1, 0.05/1, 0.075/1, and 0.1/1) were prepared by a similar synthetic procedure with the above synthesis except different Fe/Co ratios.

Material characterizations

X-ray diffraction (XRD) was carried out on a RIGAKU D/MAX2550/PC diffractometer at 40 kV and 100 mA with copper filtered $\text{K}\alpha$ radiation ($\lambda = 1.5406 \text{ \AA}$). The specific surface areas of the catalysts were measured based on the adsorption isotherms of N_2 at -196 °C using the BET method (Micromeritics ASAP2010). Transmission electron microscope (TEM) images were observed by a Hitachi HT7700.

The valence state of rhodium was determined using XPS recorded on a Thermo ESCALAB 250Xi. The X-ray source selected was monochromatized Al K α source (15 kV, 10.8 mA). Region scans were collected using 20 eV pass energy.

Electrochemical activity characterizations

All electrochemical measurements were performed in a three-electrode system with a glassy carbon electrode (GCE) as the substrate for the working electrode, a graphite rod as the counter electrode and a saturated calomel electrode as the reference electrode. The reference electrode was calibrated with respect to a reversible hydrogen electrode before each experiment. The glassy carbon electrode was pre-polished using 0.05 μm alumina and distilled water. To prepare the working electrode, 2 mg of the catalyst was dispersed in a 0.2 mL mixed solvent of ethanol and Nafion (1 wt%) and sonicated to obtain a homogeneous ink. 8 μL of the catalyst ink was drop-casted on the glassy carbon electrode and dried at room temperature (catalyst loading: 1.127 $\text{mg}\cdot\text{cm}^{-2}$).

For OER, the working electrode was first activated by steady-state cyclic voltammetry (CV) performed in the potential range from 1.0 to 1.6 V vs RHE at a scan rate of 50 mV s^{-1} for 50 cycles. Linear scan voltammetry (LSV) curves were then collected at a scan rate of 5 mV s^{-1} . All of the potentials in the LSV polarization curves were with 90% iR compensation unless specifically illustrated. The measurement error was within 10%.

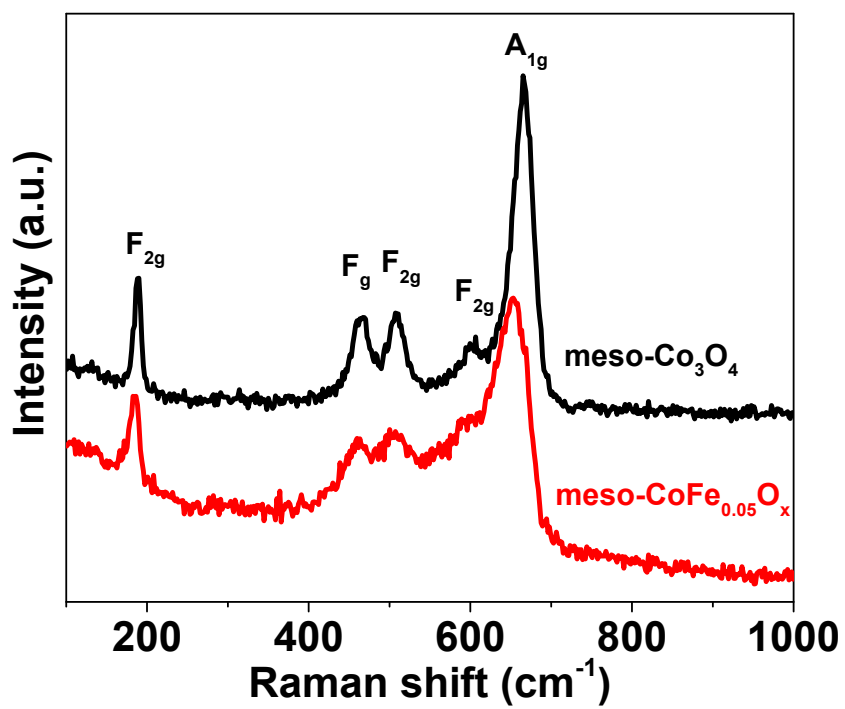


Fig. S1. Raman spectra of meso-Co₃O₄ and meso-CoFe_{0.05}O_x.

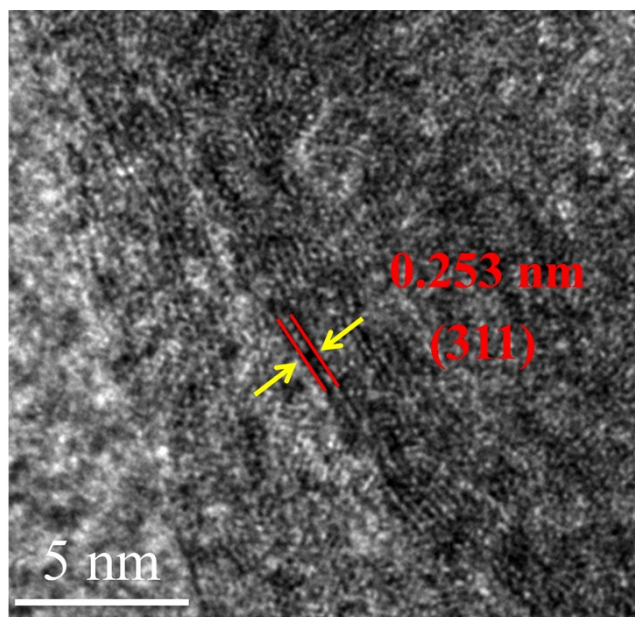


Fig. S2. HRTEM image of meso-CoFe_{0.05}O_x.

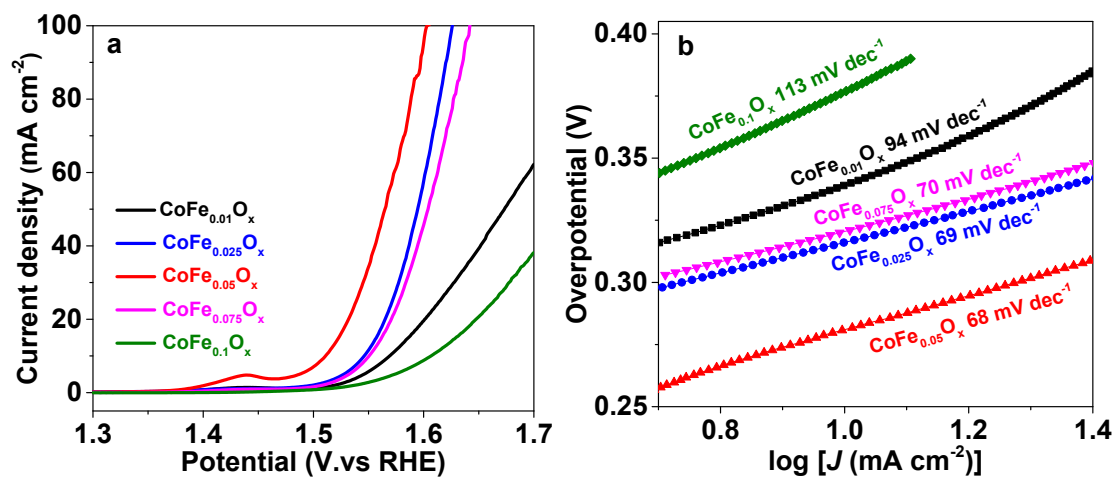


Fig. S3. (a) OER polarization curves. (b) Tafel plots.

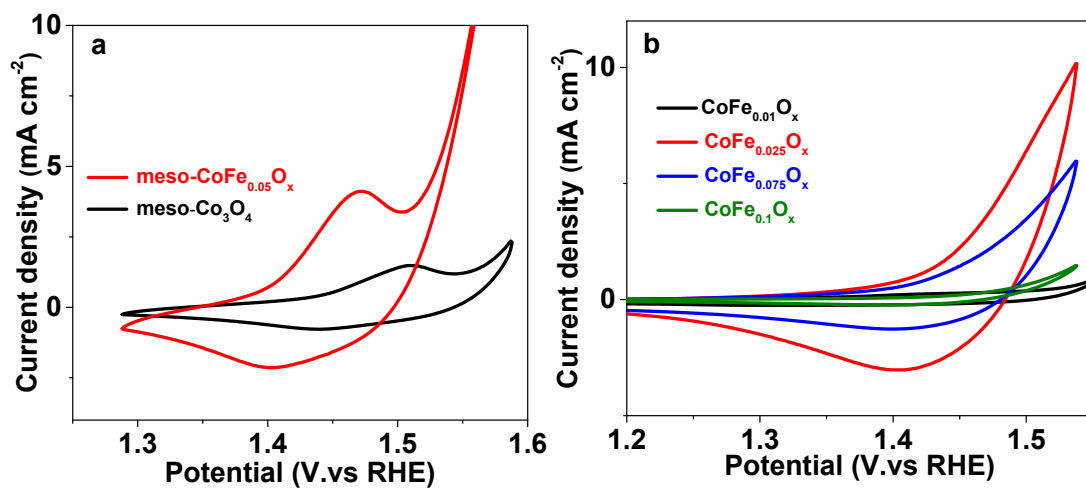


Fig. S4. (a) CVs of meso-CoFe_{0.05}O_x and meso-Co₃O₄, (b) CVs of meso-CoFenO_x.

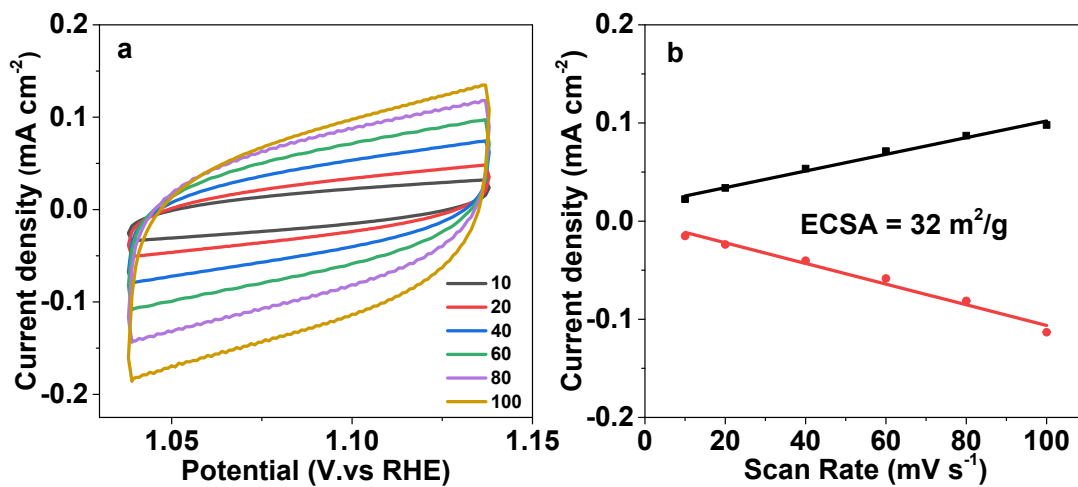


Fig. S5. (a) CVs of the meso-CoFe_{0.05}O_x measured in a non-Faradaic region at different scan rate. (b) The cathodic and anodic currents measured as a function of the scan rate.

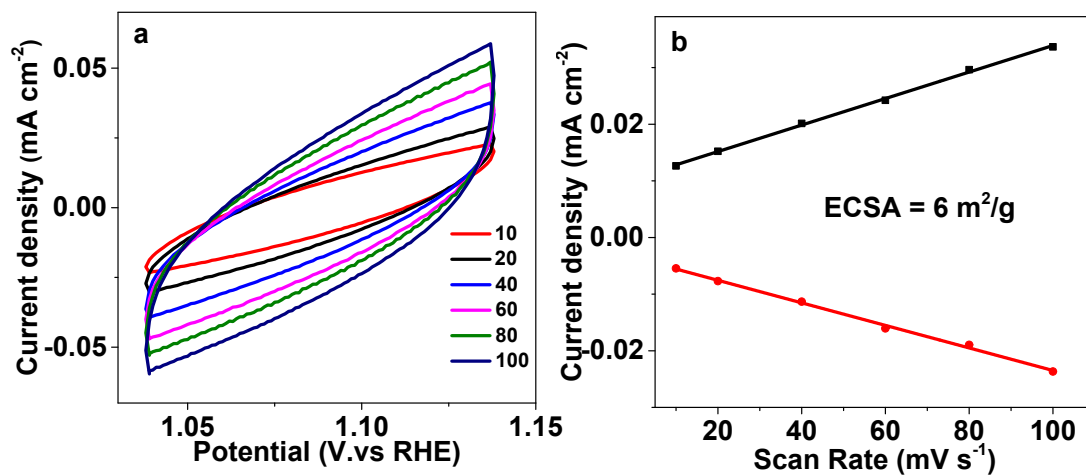


Fig. S6. (a) CVs of the commercial Co_3O_4 measured in a non-Faradaic region at different scan rate. (b) The cathodic and anodic currents measured as a function of the scan rate.

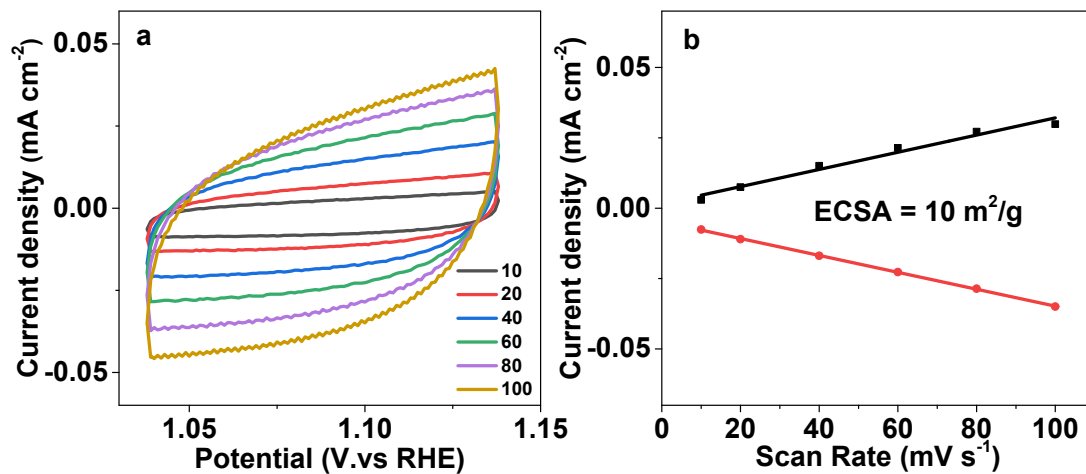


Fig. S7. (a) CVs of the meso-Co₃O₄ measured in a non-Faradaic region at different scan rate. (b) The cathodic and anodic currents measured as a function of the scan rate.

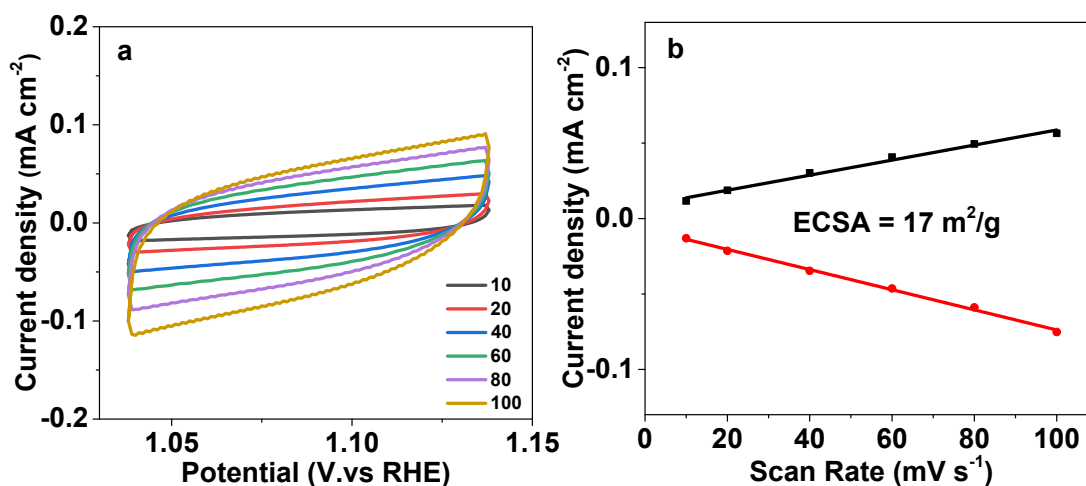


Fig. S8. (a) CVs of the meso-CoFe_{0.01}O_x measured in a non-Faradaic region at different scan rate. (b) The cathodic and anodic currents measured as a function of the scan rate.

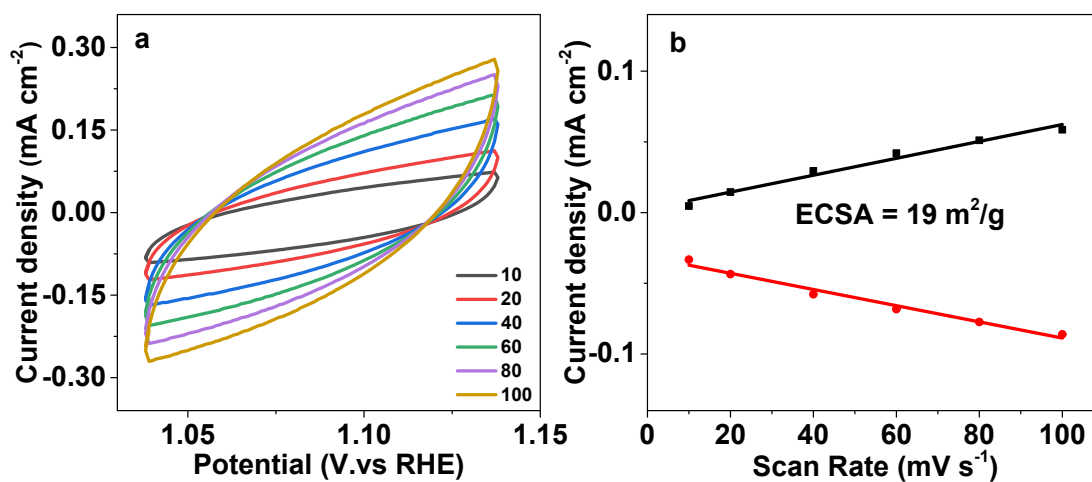


Fig. S9. (a) CVs of the meso-CoFe_{0.025}O_x measured in a non-Faradaic region at different scan rate. (b) The cathodic and anodic currents measured as a function of the scan rate.

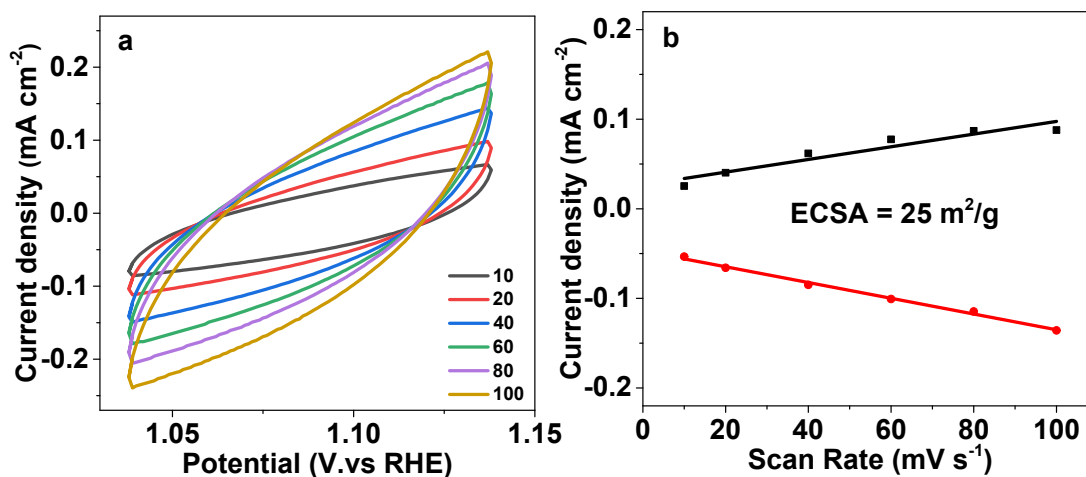


Fig. S10. (a) CVs of the meso-CoFe_{0.075}O_x measured in a non-Faradaic region at different scan rate. (b) The cathodic and anodic currents measured as a function of the scan rate.

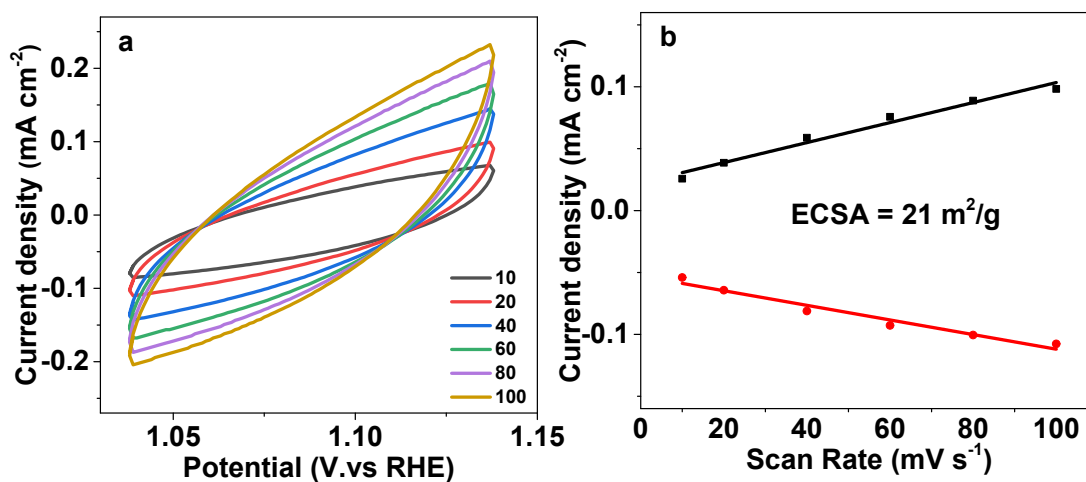


Fig. S11. (a) CVs of the meso-CoFe_{0.1}O_x measured in a non-Faradaic region at different scan rate. (b) The cathodic and anodic currents measured as a function of the scan rate.

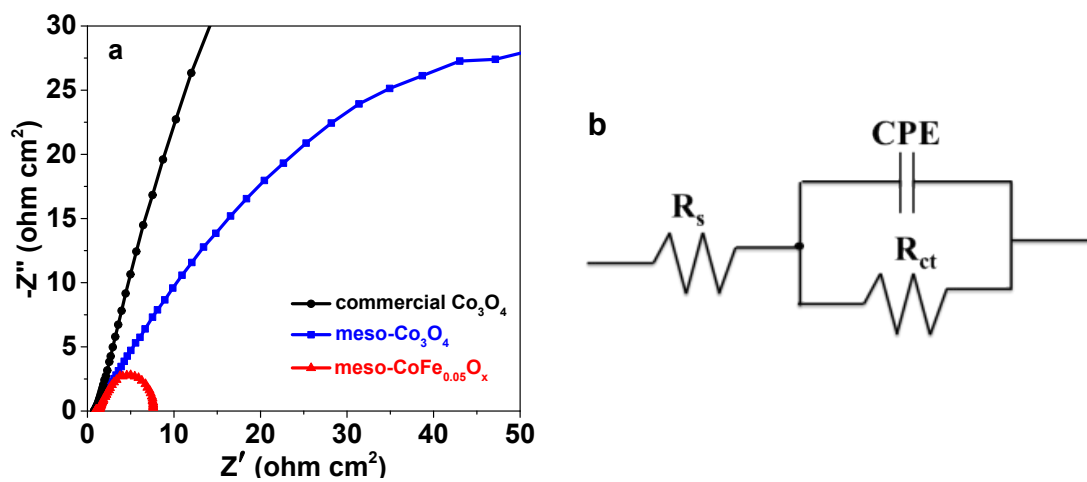


Fig. S12. (a) Nyquist plots of the EIS test. (b) The equivalent circuit used for fitting the Nyquist plots.

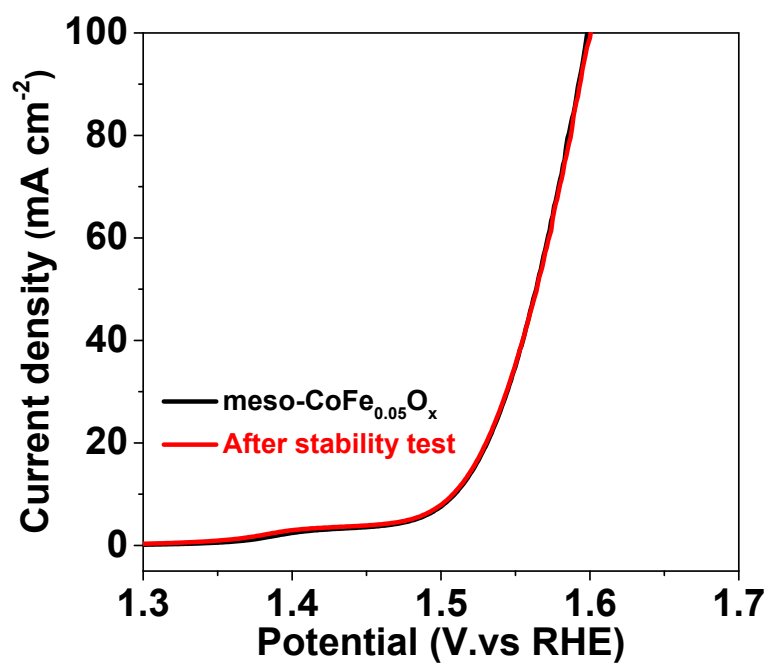


Fig. S13. OER polarization curves of the meso-CoFe_{0.05}O_x before and after stability test in 1 M KOH.

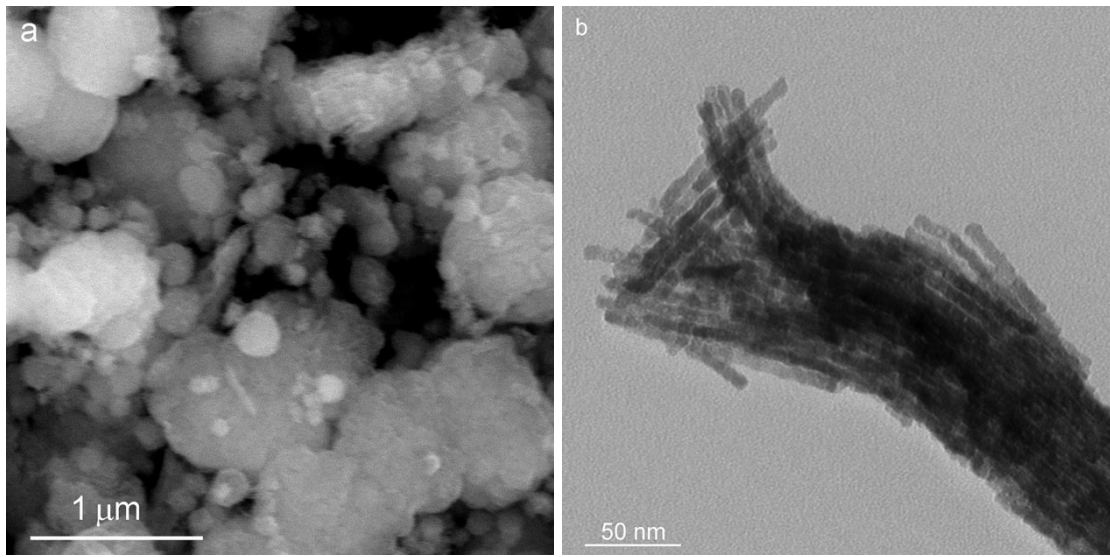


Fig. S14. (a) SEM image and (b) TEM image of meso-CoFe_{0.05}O_x after OER.

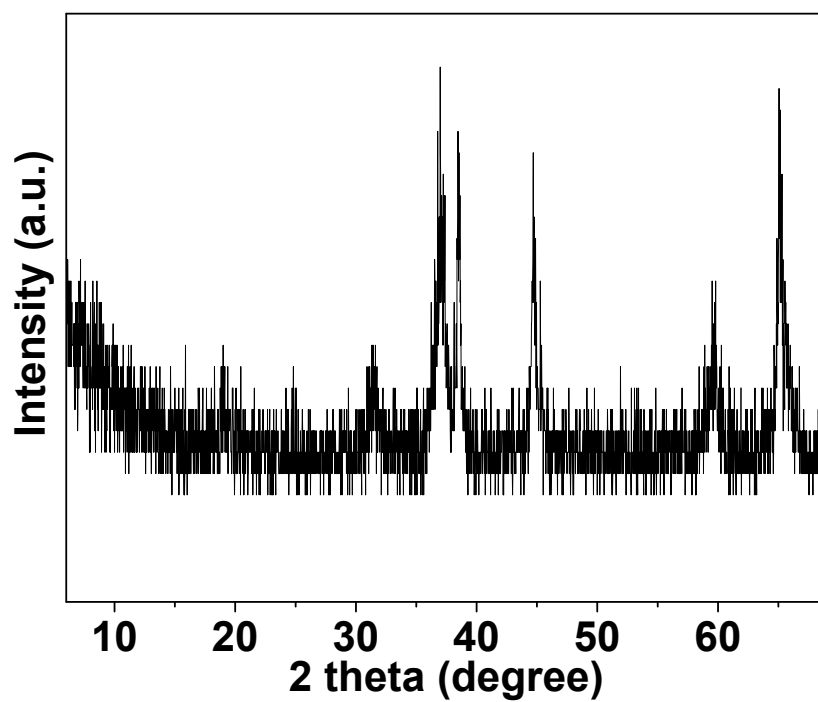


Fig. S15. XRD patterns of meso-CoFe_{0.05}O_x after OER.

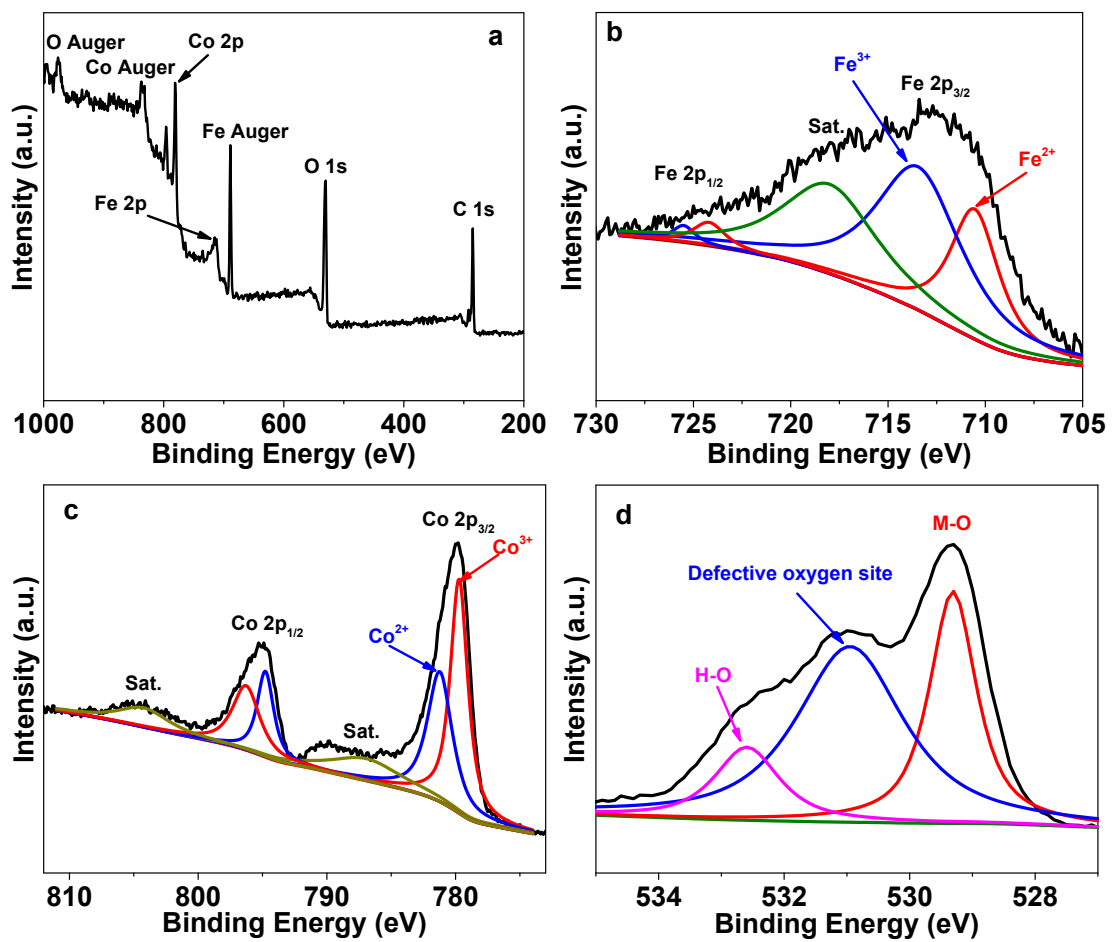


Fig. S16. XPS survey spectrum (a), and high-resolution XPS spectra of Fe 2p (b), Co 2p (c), and O 1s (d) of after the OER meso-CoFe_{0.05}O_x.

Table S1. Comparison of OER performance of meso-CoFe_{0.05}O_x with results in recent literature

| Catalyst | Electrolyte | $\eta@10$ (mV) | mA cm ⁻² | Tafel slope (mV dec ⁻¹) | Ref. |
|--|-------------|-------------------|------------------------|---|-----------|
| meso-CoFe _{0.05} O _x | 1 M KOH | 280 | | 72 | This work |
| NiFe@C | 1 M KOH | 345 | | 57 | 2 |
| CoFeP | 1 M KOH | 350 | | 59 | 3 |
| Fe-Co ₃ O ₄ /CNTs | 1 M KOH | 300 | | 54 | 4 |
| Fe-MoO ₂ /MoO ₃ /ENF | 1 M KOH | 310 | | 84.2 | 5 |
| FCPS-1:2 | 1 M KOH | 365 | | 92 | 6 |
| Co _{0.17} Fe _{0.79} P/NC | 1 M KOH | 299 | | 44 | 7 |
| P _{8.6} -Co ₃ O ₄ /NF | 1 M KOH | 400 | | 60 | 8 |
| NiFeOP | 1 M KOH | 310 | | 43.1 | 9 |
| FeNi ₃ /NiFeO _x | 1 M KOH | 246 | | - | 10 |
| FeCo/Co ₂ P@NPCF | 1 M KOH | 330 | | 61 | 11 |
| NiCo ₂ O ₄ | 1 M KOH | 420 | | - | 12 |
| BC/Co ₃ O ₄ | 1 M KOH | 310 | | 56.8 | 13 |
| PS@Co(OH) ₂ | 1 M KOH | 352 | | 80 | 14 |
| CoFeBO NS. | 1 M KOH | 240 | | 53 | 15 |
| Pt- α Fe ₂ O ₃ /NF | 1 M KOH | - | | 50.3 | 16 |
| CuCo ₂ S ₄ /CC | 1 M KOH | 280 | | 143 | 17 |

References

- 1 B. Liu, H. Liu, C. Wang, L. Liu, S. Wu, J. Guan and Q. Kan, *Applied Catalysis A: General*, 2012, **443-444**, 1-7.
- 2 S.-W. Park, I. Kim, S.-I. Oh, J.-C. Kim and D.-W. Kim, *J. Catal.*, 2018, **366**, 266-274.
- 3 Y. Du, H. Qu, Y. Liu, Y. Han, L. Wang and B. Dong, *Appl. Surf. Sci.*, 2019, **465**, 816-823.
- 4 H. Begum and S. Jeon, *Int. J. Hydrogen Energy*, 2018, **43**, 5522-5529.
- 5 J. Chen, Q. Zeng, X. Qi, B. Peng, L. Xu, C. Liu and T. Liang, *Int. J. Hydrogen Energy*, 2020, **45**, 24828-24839.
- 6 J. Tong, C. Li, L. Bo, X. Guan, Y. Wang, D. Kong, H. Wang, W. Shi and Y. Zhang, *Int. J. Hydrogen Energy*, 2021, **46**, 3354-3364.
- 7 J. Chen, Y. Zhang, H. Ye, J.-Q. Xie, Y. Li, C. Yan, R. Sun and C.-P. Wong, *ACS Appl. Energy Mater.*, 2019, **2**, 2734-2742.
- 8 Z. Wang, H. Liu, R. Ge, X. Ren, J. Ren, D. Yang, L. Zhang and X. Sun, *ACS Catal.*, 2018, **8**, 2236-2241.
- 9 J. Chen, Z. Guo, Y. Luo, M. Cai, Y. Gong, S. Sun, Z. Li and C.-J. Mao, *ACS Sustain. Chem. Eng.*, 2021, **9**, 9436-9443.
- 10 X. Yan, L. Tian, K. Li, S. Atkins, H. Zhao, J. Murowchick, L. Liu and X. Chen, *Adv. Mater. Interfaces*, 2016, **3**, 1600368.
- 11 Q. Shi, Q. Liu, Y. Ma, Z. Fang, Z. Liang, G. Shao, B. Tang, W. Yang, L. Qin

- and X. Fang, *Adv. Energy Mater.*, 2020, **10**, 1903854.
- 12 X. Gao, H. Zhang, Q. Li, X. Yu, Z. Hong, X. Zhang, C. Liang and Z. Lin, *Angew. Chem. Int. Ed.*, 2016, **55**, 6290-6294.
- 13 L. Zou and Q. Xu, *Chem. Asian J.*, 2020, **15**, 490-493.
- 14 L. Hang, Y. Sun, D. Men, S. Liu, Q. Zhao, W. Cai and Y. Li, *J. Mater. Chem. A*, 2017, **5**, 11163-11170.
- 15 B. Liu, N. Zhang and M. Ma, *J. Mater. Chem. A*, 2017, **5**, 17640-17646.
- 16 B. Ye, L. Huang, Y. Hou, R. Jiang, L. Sun, Z. Yu, B. Zhang, Y. Huang and Y. Zhang, *J. Mater. Chem. A*, 2019, **7**, 11379-11386.
- 17 C. Ren, Y. Chen, L. Du, Q. Wang, L. Li and G. Tian, *ChemElectroChem*, 2021, **8**, 1134-1140.
- 18 T.-T. H. Nguyen, J. Lee, J. Bae and B. Lim, *Chemistry – A European Journal*, 2018, **24**, 4724-4728.